

Finite temperature study of correlations in bilayer band-insulator

Yogeshwar Prasad^{1,*}

¹Center for Condensed Matter Theory, Department of Physics,
Indian Institute of Science, Bangalore 560012, India

(Dated: November 22, 2022)

We perform the finite-temperature determinant quantum Monte Carlo simulation for the attractive Hubbard model on the half-filled bilayer square lattice. Recent progress on optical lattice experiments lead us to investigate various single-particle properties such as momentum distribution and double occupancies which should be easily measured in cold-atom experiments. The pair-pair and the density-density correlations have been studied in detail, and through finite-size scaling, we show that there is no competing charge density wave order in the bilayer band-insulator model and that the superfluid phase is the stable phase for the interaction range $|U|/t = 5 - 10$. We show the existence of two energy scales in the system as we increase the attractive interaction, one governing the phase coherence and the other one corresponding to the molecule formation. In the end, we map out the full $T - U$ phase diagram and compare the T_c obtained through the mean-field analysis. We observe that the maximum $T_c/t (= 0.27)$ occurs for $|U|/t = 6$, which is roughly twice the reported T_c of the single-layer attractive Hubbard model.

I. INTRODUCTION

The half-filled attractive Hubbard model (AHM), at low temperatures, shows the s -wave superfluidity with a BEC-BCS crossover along with the charge density wave (or pair density wave) [1]. In the weak-coupling regime ($U \ll t$), fermions of opposite spin and same momentum state form loosely bound Cooper pairs and go to the BCS state at the critical temperature T_c , which increases with $|U|/t$. As we go towards the strong-coupling regime ($U \gg t$), the strong interactions between the particles lead to the formation of the bound pairs that condense to form a BEC state at T_c , which decreases as $t^2/|U|$. The fermionic pairs in the BEC state can be regarded as the hard-core bosons, and the tunneling of the pairs is dominated by the second-order tunneling $t^2/|U|$.

The advancement in the field of cold atoms has generated a lot of interest in the condensed matter community due to a control over various parameters such as tuning the interaction between particles by the Feshbach resonance, tuning the hopping between lattice sites by laser intensity, and so on. The lowest temperature that has been achieved so far in experiments on the AHM is $T \sim 0.4t$ [2]. Earlier theoretical work on half-filled AHM has shown $T_c \sim 0.13t$ for $|U|/t = 8$ [3], whereas the maximum $T_c \sim 0.17t$ at density $n = 0.7$ and $|U|/t = 4$ has been reported [4, 5]. The process to lower the temperature experimentally in optical lattice systems has been hampered by the cooling problem (entropy issues) [4, 6–9]. Recent progress made in the experiments towards the realization of the attractive Hubbard model has been of great interest [2, 10]. There have been some theoretical attempts to “increase” the characteristic temperature T_c which can be achieved experimentally [11, 12]. In this work, we focus on the bilayer attractive Hub-

bard model band-insulator model discussed in Ref. [11]. The model is a bilayer square lattice model, as shown in Fig. 1. Both layers have been hybridized by the coupling t_h . The hoppings in both layers were taken to be opposite to each other such that the in-plane energy dispersions in the two layers are of the *opposite* signs, i.e., $\epsilon_A(\mathbf{k}) = -\epsilon_B(\mathbf{k}) \equiv \epsilon(\mathbf{k})$. The idea is to start with a low entropy state and explore the possibility of realizing a superfluid. At half filling, for a finite t_h and for small values of $|U|$, the system is in the normal band-insulator state. With the increase in the on-site attractive interaction $|U|$, a quantum phase transition occurs at $|U_c|$, ushering in a superfluid state. Detailed analysis including Gaussian fluctuations and variational Monte Carlo (VMC) calculations establish that there are no competing orders such as an intervening charge density wave (CDW) and confirm that the superfluid state is stable at $T = 0$ [11]. Band-insulator-superfluid transitions have been studied

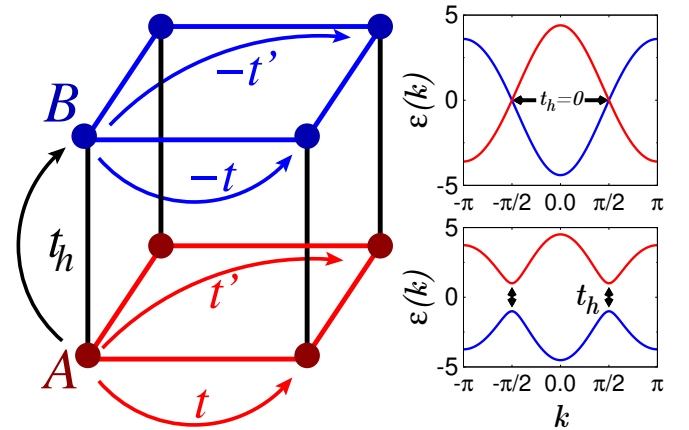


Figure 1. Schematic of the bilayer band insulator. Nearest-neighbor hopping t and next-nearest-neighbor hopping t' in layer A is opposite to that of layer B of the square lattice. Both layers have been hybridized by hopping t_h . The right panel shows the energy dispersion for $t_h = 0$ and $t_h \neq 0$.

* yogeshwar@iisc.ac.in

earlier in other contexts [13, 14]. The quantum Monte Carlo studies for the attractive Hubbard model have been done in the past for single layer [15–18] as well as bilayer [19] square lattices. These simulations motivated us to analyze the bilayer band-insulator model using the determinant quantum Monte Carlo (DQMC) technique.

We use the DQMC technique [20, 21] to study the equilibrium properties of the bilayer band-insulator model with attractive Hubbard interaction. A key point with this model is that there is no sign problem for the attractive on-site interaction. So it is possible to explore the physics of this bilayer model at low temperatures. We have examined the nature of the pairing correlations for our model through DQMC, which provides an approximation-free solution of the discussed model. In the end, we perform the scaling analysis and estimate T_c through the finite-size scaling (FSS).

II. MODEL AND COMPUTATIONAL METHOD

We start with the Hamiltonian of the bilayer square lattice model, $\mathcal{H} = \mathcal{H}_K + \mathcal{H}_U$, where

$$\begin{aligned} \mathcal{H}_K = & \overbrace{-t \sum_{\langle \mathbf{ij} \rangle, \sigma} (a_{\mathbf{i}\sigma}^\dagger a_{\mathbf{j}\sigma} + h.c.) - t' \sum_{\langle \mathbf{ii}' \rangle, \sigma} (a_{\mathbf{i}\sigma}^\dagger a_{\mathbf{i}'\sigma} + h.c.)}^{\text{A-layer}} \\ & + \overbrace{t \sum_{\langle \mathbf{ij} \rangle, \sigma} (b_{\mathbf{i}\sigma}^\dagger b_{\mathbf{j}\sigma} + h.c.) + t' \sum_{\langle \mathbf{ii}' \rangle, \sigma} (b_{\mathbf{i}\sigma}^\dagger b_{\mathbf{i}'\sigma} + h.c.)}^{\text{B-layer}} \\ & - \underbrace{\sum_{\mathbf{i}, \sigma} t_h(\mathbf{i}) (a_{\mathbf{i}\sigma}^\dagger b_{\mathbf{i}\sigma} + h.c.) - \mu \sum_{\mathbf{i}, \sigma} (a_{\mathbf{i}\sigma}^\dagger a_{\mathbf{i}\sigma} + b_{\mathbf{i}\sigma}^\dagger b_{\mathbf{i}\sigma})}_{\text{A-B Layer hybridization}}; \\ \mathcal{H}_U = & \underbrace{-U \sum_{\mathbf{i}} (a_{\mathbf{i}\uparrow}^\dagger a_{\mathbf{i}\downarrow}^\dagger a_{\mathbf{i}\downarrow} a_{\mathbf{i}\uparrow} + b_{\mathbf{i}\uparrow}^\dagger b_{\mathbf{i}\downarrow}^\dagger b_{\mathbf{i}\downarrow} b_{\mathbf{i}\uparrow})}_{\text{Interaction Hamiltonian}} \end{aligned} \quad (1)$$

$$t_{\mathbf{ij}\alpha\gamma} = \begin{cases} -t & \text{if } \mathbf{i} \text{ and } \mathbf{j} \text{ are the } nn \text{ for } (\alpha, \gamma) = (1, 1) \\ -t' & \text{if } \mathbf{i} \text{ and } \mathbf{j} \text{ are the } nnn \text{ for } (\alpha, \gamma) = (1, 1) \\ t & \text{if } \mathbf{i} \text{ and } \mathbf{j} \text{ are the } nn \text{ for } (\alpha, \gamma) = (2, 2) \\ t' & \text{if } \mathbf{i} \text{ and } \mathbf{j} \text{ are the } nnn \text{ for } (\alpha, \gamma) = (2, 2) \\ -t_h & \text{if } \mathbf{i} \text{ and } \mathbf{j} \text{ are the } nn \text{ for } (\alpha, \gamma) = (1, 2) \text{ or } (2, 1) \\ 0 & \text{otherwise.} \end{cases} \quad (4)$$

where nn represents the nearest neighbors, while nnn represents the next-nearest neighbors. After applying the Hubbard-Stratonovich transformation for the bilayer band-insulator model, the elements of the matrix \mathbb{V} and the chemical potential in the kinetic energy term are modified to

$$\begin{aligned} \mathbb{V}_{\mathbf{ij}\alpha\gamma}^\sigma &= -\frac{\lambda s_{\mathbf{i}}}{\Delta\tau} \delta_{\mathbf{ij}} \delta_{\alpha\gamma}, \\ \tilde{\mu} &= \mu + \frac{|U|}{2}. \end{aligned} \quad (5)$$

Hence, at half filling, we have $\tilde{\mu} = 0$. We calculate various single-particle quantities such as the momentum

in the presence of the on-site Hubbard interaction (“ $-U$ ”). The first term \mathcal{H}_K represents the hopping (kinetic energy) of the fermions and the latter represents the interaction energy when the two fermions occupy the same site. We choose the nearest-neighbor hopping $t = 1$ to set our unit of energy. We express all other energy scales t_h, U, T and μ in terms of the energy scale t . We fix the hybridization hopping $t_h/t = 0.6$ throughout this work and studied the properties of our model at half-filling on a bilayer square lattice with $\mathcal{N} = 2 \times L^2$ sites with periodic boundary conditions. Here L represents the number of sites in each direction of the square lattice. At half-filling (one fermion per site), due to particle-hole symmetry in our system, $\mu = 0$.

In the DQMC simulations, we chose the imaginary-time interval $\Delta\tau = 1/20$. Following the steps of the DQMC algorithm [20, 21], we perform the Trotter-Suzuki decomposition to separate the kinetic and interaction energy exponentials. For the proposed bilayer band-insulator model, the kinetic and the interaction exponentials will have the following expressions:

$$\begin{aligned} e^{-\Delta\tau\mathcal{K}} &= \prod_{\sigma} e^{-\Delta\tau \sum_{\alpha\gamma} \sum_{\langle \mathbf{ij} \rangle} (c_{\mathbf{i}\alpha\sigma}^\dagger \mathbb{K}_{\mathbf{ij}\alpha\gamma}^\sigma c_{\mathbf{j}\gamma\sigma} + \text{h.c.})} \\ e^{-\Delta\tau\mathcal{V}} &= e^{\Delta\tau \sum_{\alpha} \sum_{\mathbf{i}} (-U n_{\mathbf{i}\uparrow}^\alpha n_{\mathbf{i}\downarrow}^\alpha + \mu(n_{\mathbf{i}\uparrow} + n_{\mathbf{i}\downarrow}))} \end{aligned} \quad (2)$$

where (α, γ) correspond to the layers of the bilayer system and $c_\alpha(c_\alpha^\dagger)$ is equivalent to the operators $a(a^\dagger)$ and $b(b^\dagger)$ for $\alpha = 1$ and 2 , respectively. \mathbb{K} is the kinetic energy matrix whose elements are given by

$$\mathbb{K}_{\mathbf{ij}\alpha\gamma}^\sigma = t_{\mathbf{ij}\alpha\gamma} - \mu \delta_{\mathbf{ij}} \delta_{\alpha\gamma}, \quad (3)$$

with

distribution, kinetic energy, and double occupancy, two-particle correlations such as pair-pair correlations and density-density correlations using the DQMC simulation. For each data point at the given value of the inverse temperature β , the interaction $|U|$, and the lattice size $L = 10 - 16$, the simulations were carried out with 1000 – 10000 warm-up sweeps and 10000 – 50000 measurement sweeps of the space-time lattice. These measurement sweeps were divided into 20 bins and thus the statistical average over these 20 bins has been reported here.

III. SINGLE PARTICLE PROPERTIES

The mean-field analysis and the Gaussian fluctuation theory suggest that the bilayer band-insulator model undergoes a second-order phase transition at some critical value of the attractive interaction $|U_c|$ [11]. The fermions start to form pairs as we tune the on-site attractive interaction through Feshbach resonance. In the strong-coupling limit ($|U| \gg t$), these pairs get tightly bound, forming a molecule (boson). Thus, by tuning the interaction, we go from a band-insulating state to a loosely bound state of Cooper pairs and then to a tightly bound molecule-forming state, implying that there is a smooth *BCS*–*BEC* crossover extending from a small to a large value of the interactions. Hence, the ground state of the system evolves continuously from a *BCS* state (where fermions with opposite spins form loose pairs of plane waves with opposite momenta) to a *BEC* state of bosonic molecules (where fermions with opposite spin form tightly bound pairs) when $|U|$ is increased beyond $|U_c|$.

A. Momentum Distribution

The Green's function is a fundamental quantity in DQMC where it is used in various updation processes. The momentum distribution can be obtained directly from the Green's function via Fourier transform of the equal-time Green's function $G_{ij\alpha\beta} = \langle c_{i\alpha\sigma} c_{j\beta\sigma}^\dagger \rangle$ as

$$n_\alpha(\mathbf{q}) = 1 - \frac{1}{2N_\alpha} \sum_{\mathbf{i}, \mathbf{j}, \sigma} e^{i\mathbf{q} \cdot \mathbf{l}_{ij}^\alpha} \langle c_{i\alpha\sigma} c_{j\alpha\sigma}^\dagger \rangle \quad (6)$$

where $\mathbf{l}_{ij}^\alpha = \mathbf{l}(\mathbf{i}, \alpha) - \mathbf{l}(\mathbf{j}, \alpha)$ and $N_\alpha (= L^2)$ represents the number of sites in the α th layer.

Figure 2 shows the momentum distribution of our bilayer square lattice around the irreducible part of the Brillouin zone (BZ) for various system sizes [Fig. 2(a)], at different temperatures [Fig. 2(b)], and for different interactions $|U|$ [Figs. 2(c) and 2(d)]. At $|U| = 0$ and at half filling, $n_1(\mathbf{q})$ [$n_2(\mathbf{q})$] = 1(0) inside and $n_1(\mathbf{q})$ [$n_2(\mathbf{q})$] = 0(1) outside a square with vertices $(\pi, 0)$, $(0, \pi)$, $(-\pi, 0)$, and $(0, -\pi)$ within the BZ. Figure 2(a) shows that the momentum distribution has a weak lattice size dependence and its resolution increases with L . In Fig. 2(b), we show that the $n(\mathbf{q})$'s converge to their respective low-temperature values as $\beta t > W/t$, where $W (= 8.8 t)$ is the bandwidth of the noninteracting energy dispersion. We find that the smearing due to the finite-temperature effects is very small above $\beta t = 8.8$. In Fig. 2(c), we see a sharp Fermi surface at weak interaction $|U|$ as the momentum cuts across the Fermi surface at $\mathbf{q} = (\pi/2, \pi/2)$, whose enlarged plot is shown in Fig. 2(d), which focuses on the region near the Fermi surface point $(\pi/2, \pi/2)$. It shows that the distribution broadens out as the interaction $|U|$ increases. In Fig. 3, we show a sequence of color contour plots for the lattice size $L = 16$ at $|U|/t = 1, 5$, and 8.

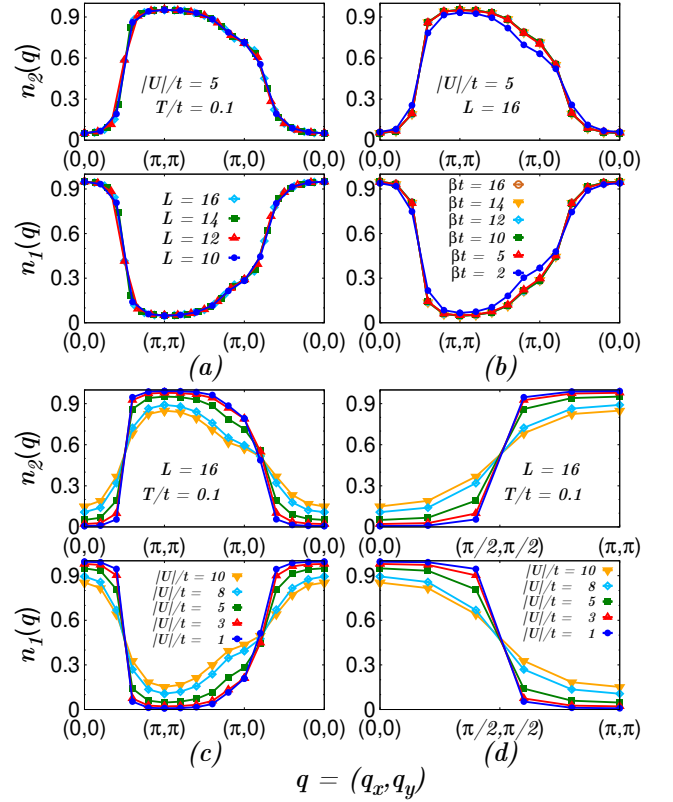


Figure 2. Momentum distributions. (a) The momentum distributions are shown for the interaction strengths $|U|/t = 5$ and the inverse temperature $\beta t = 10$ for various system sizes. $n_1(\mathbf{q})$ and $n_2(\mathbf{q})$ are the momentum distributions corresponding to layer A and B, respectively. It shows weak lattice size dependence and the resolution increases with L . (b) The $n(\mathbf{q})$'s converge to their low temperature value as $\beta t > W/t$. Here, $|U|/t = 5$ and the system size $L = 16$. (c) The momentum distributions for various attractive interactions ranging from $|U|/t = 1$ to 8; (d) the enlarged region, cut perpendicular to the Fermi surface at $(\pi/2, \pi/2)$, of (c). We see a sharp Fermi surface at weak interaction $|U|$ as the momentum cuts across the Fermi surface at $\mathbf{q} = (\pi/2, \pi/2)$ and it broadens out as $|U|/t$ increases.

B. Pair Formation

The existence of the molecule formation along the *BCS*–*BEC* crossover with the increase in the interaction strength $|U|$ comes from the evolution of the double occupancy (density of on-site pairs), which can also be measured in experiments with ultracold fermions [22]. The double occupancy D can be defined as

$$D = \frac{1}{N} \sum_{i\alpha} \langle n_{i\uparrow}^\alpha n_{i\downarrow}^\alpha \rangle \quad (7)$$

where the summation i runs over the number of sites for layer α for both layers $\alpha = 1$ and 2, and $N (= 2L^2)$ represents the total number of sites.

In the noninteracting limit ($|U|/t = 0$), both spin-up and spin-down particles are uncorrelated so $\sum_{i\alpha} \langle n_{i\uparrow}^\alpha n_{i\downarrow}^\alpha \rangle / N = \sum_{i\alpha} \langle n_{i\uparrow}^\alpha \rangle \langle n_{i\downarrow}^\alpha \rangle / N = 1/4$ at half filling. As we increase the attractive interaction by tuning the scattering rate, the spin-up and spin-down particles

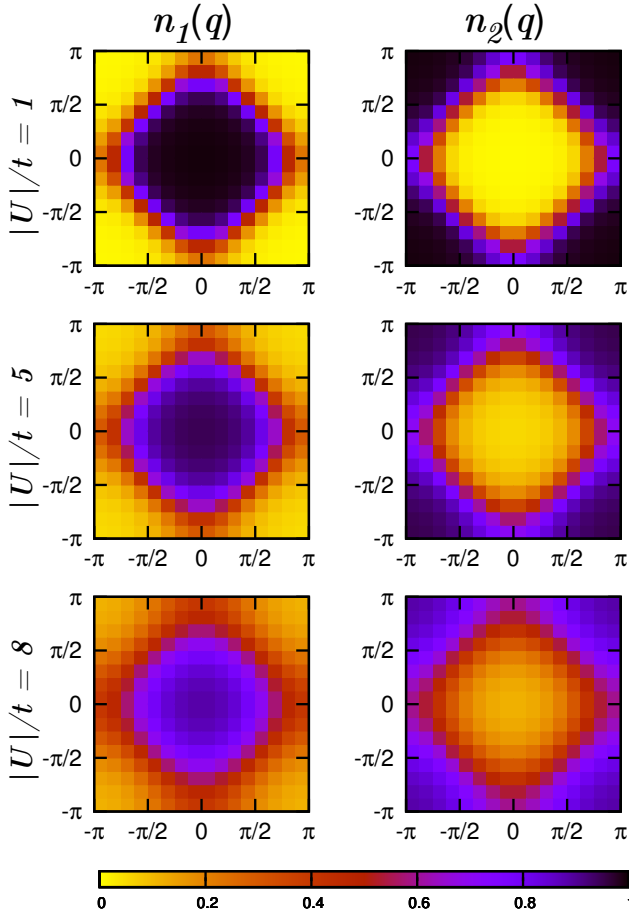


Figure 3. Color contour plot depiction of the momentum distributions. $n_1(\mathbf{q})$ and $n_2(\mathbf{q})$ at half filling for $|U|/t = 1, 5$, and 8 . The lattice size $= 2 \times 16 \times 16$ and the inverse temperature $\beta t = 10$.

become correlated. In the strong-coupling limit ($|U|/t \rightarrow \infty$), the large attractive interaction locks the fermions in bound on-site pairs and hence they form a charge density wave where the fermion pairs occupy alternate sites of the bilayer lattice at half filling to minimize the energy by a virtual hopping process of the order of $t^2/|U|$. In this limit, at half filling, the on-site pair density or the double occupancy will be equal to the number of up- or down-spin fermions which is 0.5 at half filling: since $n = 1$, $\sum_{i\alpha} \langle n_{i\uparrow}^\alpha n_{i\downarrow}^\alpha \rangle / N = \sum_{i\alpha} \langle n_{i\uparrow}^\alpha \rangle / N = \sum_{i\alpha} \langle n_{i\downarrow}^\alpha \rangle / N = 1/2$.

In Fig. 4(a), we have plotted the rescaled double occupancy,

$$\tilde{D} = \frac{D - \langle n_{i\uparrow}^\alpha \rangle^2}{\langle n_{i\uparrow}^\alpha \rangle - \langle n_{i\uparrow}^\alpha \rangle^2} = (4D - 1) \quad (8)$$

as a function of temperature T for various interaction strengths. As the attractive interaction increases from zero to infinity, the rescaled double occupancy increases from 0 to 1 . In the $|U| \rightarrow \infty$ limit, all the fermions get paired up and hence \tilde{D} approaches the value 1 . The rescaled double occupancy reaches upto 0.8 at $|U|/t = 8$, which is an indication of the formation of bosonic

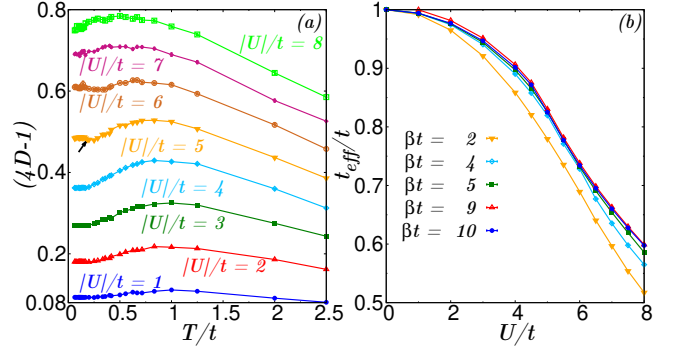


Figure 4. The evolution of the rescaled double occupancy with the temperature T/t for various interaction strengths $|U|/t$. The system size is $L = 16$. The black arrow marks the transition temperature $T_c/t = 0.17$ at $|U|/t = 5$, estimated from the finite-size scaling analysis. The rescaled double occupancy reaches up to 0.8 at $|U|/t = 8$, which is an indication of the molecule (tightly bound pairs) formation. A local maxima has been observed as we go from the high-temperature to the low-temperature regime at the intermediate-temperature scale $T/t \sim 1$. (b) Effective hopping: as the interaction energy $|U|$ increases, the effective hopping declines. The rate of decrease of the effective hopping with the increase in the interaction strength is the same for all $\beta t > W/t(8.8/t)$. Here we show t_{eff}/t for $L = 16$ for different values of inverse temperature βt .

molecules (tightly bound pairs of fermions of opposite spins). In the high-temperature limit ($T/t \gg 1$), independent of the interaction strength, the double occupancy approaches the noninteracting values, i.e., 0.25 in the half-filled case. As we decrease the temperature, the fermions start to pair up due to the increasing effect of the attractive interaction. Hence the double occupancy increases with the decrease in temperature T . We observe a local maxima as we go from the high-temperature to the low-temperature regime, implying the increase in the double occupancy with the decrease in the temperature. We see the local maxima at the intermediate temperature scale ($T/t \sim 1$), where the kinetic energy competes with the on-site interaction and destabilizes the double occupancy in the weak- and intermediate-coupling regimes. So the double occupancy decreases a little and saturates in the weak-coupling regime, after reaching its ground-state value as $T/t \rightarrow 0$. But after a certain critical interaction strength $|U_c|$, we observe that as we decrease the temperature further, the double occupancy increases again after a critical temperature T_c and then saturates to its low-temperature value. This indicates that the system goes into a superfluid phase from the band-insulating phase at this critical interaction strength and temperature. We estimate these critical values through the scaling analysis discussed at the end of this paper.

C. Kinetic Energy

Another single-particle quantity of interest is the effective hopping, defined as

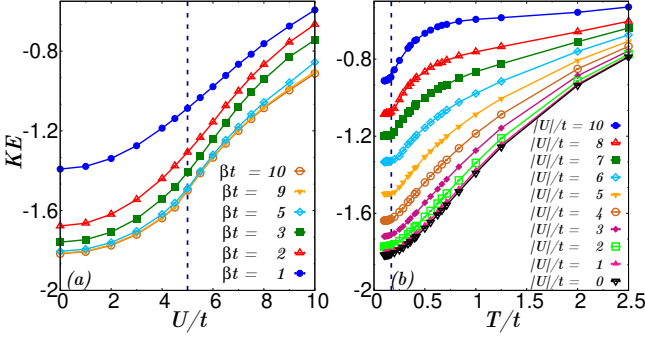


Figure 5. The evolution of the kinetic energy as a function of (a) interaction strength $|U|/t$ for various temperatures and (b) temperature T/t for different interaction strengths. The kinetic energy (KE) increases continuously with the increase in the attractive interaction, approaching its zero-temperature value for $\beta t > W/t(8.8/t)$. The evolution of KE with temperature T at weak couplings shows a similar behavior as the free-fermion case, while at strong couplings, we observe a sharp fall of the KE at low temperatures before it approaches its zero-temperature value. Here the system size is $L = 16$. In (a), the vertical dashed line shows the value of $|U_c|/t = 5$ in the ground-state, and in (b), it corresponds to $T_c/t = 0.17$ at $|U|/t = 5$.

$$\frac{t_{eff}}{t} = \frac{\langle \mathcal{H}_K \rangle_U}{\langle \mathcal{H}_K \rangle_{U=0}}, \quad (9)$$

which measures the ratio of the kinetic energy at finite $|U|$ to its value when there is no on-site interaction, i.e., $U = 0$. In Fig. 4(b), we show the effective hopping as a function of the interaction strength $|U|$ for $L = 16$ at various temperatures. As the on-site attractive interaction $|U|$ increases, the effective hopping decreases. This is due to the fact that the kinetic energy increases from larger negative value to the lower negative value with the increase in the interaction, as shown in Fig. 5(a). The rate of decrease of the effective hopping with the increase in the interaction strength is the same for all $\beta t > W/t(8.8/t)$, implying that the kinetic energy has reached its low-temperature value, as seen in Fig. 5(a). In Fig. 5(b), we show the evolution of the kinetic energy as a function of temperature T/t for different interaction strengths for a system of 512 sites. We see that the evolution of the kinetic energy with temperature T at weak couplings shows a similar behavior as the free-fermion case, while for intermediate couplings, the rate of decrease in kinetic energy with the decrease in temperature is slow as compared to the weak-coupling behavior. In the strong-coupling limit, at low temperatures, we see a sharp drop in the kinetic energy which then approaches its zero-temperature value, which is due to the reason that the kinetic energy at strong couplings is determined by the effective hopping of the paired fermions which form a bound state in this limit.

IV. TWO PARTICLE CORRELATIONS

We now turn to the two-particle properties focusing on the pair correlations in the bilayer band insulator model.

We will also discuss the density-density correlations to see the possibility of formation of the charge density wave (CDW) state at a large value of the on-site attractive interaction. We also estimate the critical strength $|U_c|$ and the critical temperature T_c through the finite-size scaling analysis.

A. Pair-Pair Correlations

We know that the long-range order (or a quasi-long-range order for a superfluid at finite temperature) in the pair-pair correlation function in the Bose-Einstein condensate state signifies a phase coherence between pairs. To study this behavior, we define the *equal-time s-wave* pairing $P_s^{\alpha\gamma}(\mathbf{i}, \mathbf{j})$ for the bilayer model as

$$P_s^{\alpha\gamma}(\mathbf{i}, \mathbf{j}) = \langle \Delta_s(\mathbf{i}, \alpha) \Delta_s^\dagger(\mathbf{j}, \gamma) + \text{h.c.} \rangle \quad (10)$$

where the local *pair-field* operator $\Delta_s(\mathbf{i}, \alpha)$, defined as

$$\Delta_s(\mathbf{i}, \alpha) = c_{\mathbf{i}, \alpha\downarrow} c_{\mathbf{i}, \alpha\uparrow}, \quad (11)$$

annihilates a *pair* of fermions on site \mathbf{i} of layer α of the bilayer-square lattice. We also define the associated pair structure factor as

$$S_s(\mathbf{q}) = \frac{1}{N} \sum_{\alpha\gamma} \sum_{\mathbf{ij}} e^{i\mathbf{q} \cdot \mathbf{l}_{ij}^{\alpha\gamma}} P_s^{\alpha\gamma}(\mathbf{i}, \mathbf{j}) \quad (12)$$

where $\mathbf{l}_{ij}^{\alpha\gamma} = \mathbf{l}(\mathbf{i}, \alpha) - \mathbf{l}(\mathbf{j}, \gamma)$.

The pair structure factor diverges linearly with the system size N when the long-range order is achieved. As the bilayer band-insulator system undergoes a finite-temperature Berezinski-Kosterlitz-Thouless (BKT) transition into a superfluid phase [11], hence for $0 < T \leq T_c$, we expect that

$$P_s(\mathbf{l}) \sim \mathbf{l}^{-\eta(T)}, \quad (13)$$

with the separation $\mathbf{l} = |\mathbf{i} - \mathbf{j}|$, where \mathbf{i}, \mathbf{j} refers to sites either from layer A or B . The critical exponent $\eta(T)$ for a BKT transition in a homogeneous system is known to increase monotonically with temperature between $\eta(0) = 0$ and $\eta(T_c) = 1/4$ [23, 24].

Thus we can obtain the finite-size scaling behavior of the *s-wave* pair structure factor upon integrating $P_s(\mathbf{l})$ over a two-dimensional system of *linear* dimension L . Hence, $S_s(\equiv S_s(\mathbf{q} = 0))$ will scale as [15]

$$L^{2-\eta(T_c)} S_s \sim f(L/\xi), \quad L \gg 1, T \rightarrow T_c^+ \quad (14)$$

with $\xi \sim \exp[A/(T - T_c)^{1/2}]$ the correlation length of the infinite system where A is of the order of unity. In the thermodynamic limit, one can recover $S_s \sim \xi^{7/4}$.

In Fig. 6, we have shown the dependence of the pair correlation function on the separation \mathbf{l} for two different lattice sizes $L = 14$ and 16 . The separation \mathbf{l} follows a trajectory along the x axis to maximal x separation $(\frac{L}{2}, 0)$ on a lattice with periodic boundary conditions, and then to $(\frac{L}{2}, \frac{L}{2})$ before returning to separation $(0, 0)$. We observe that there is no pair-pair correlation when $|U|/t = 1$ as the system is still in the band-insulating state. For $|U|/t = 5$ and 8 , there is a finite nonzero pair-pair correlation, implying the existence of the long-range

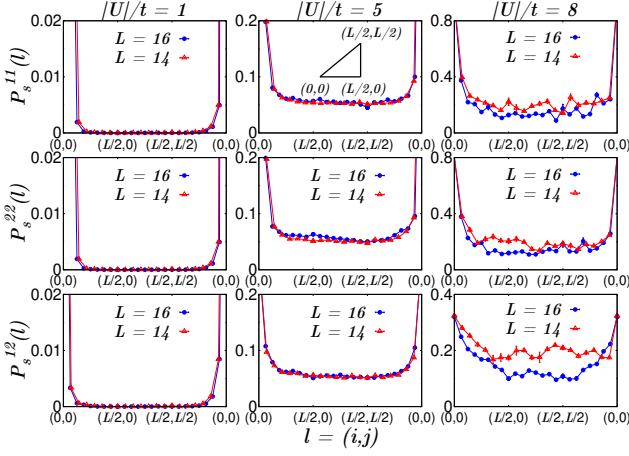


Figure 6. The dependence of the ground-state pair-pair correlation function on the separation \mathbf{l} for two different lattice sizes $L = 14$ and $L = 16$, in a bilayer band-insulator model. The separation \mathbf{l} follows a trajectory along the x axis to maximal x separation $(\frac{L}{2}, 0)$ on a lattice with periodic boundary conditions, and then to $(\frac{L}{2}, \frac{L}{2})$ before returning to separation $(0, 0)$. The correlation functions converge to a nonzero value at large separations at $|U|/t = 5$ and 8 , providing clear evidence for the long-range order. We see that the finite-size effects are modest.

order at these interactions. We see that the finite-size effects are modest.

To have a clearer understanding, in Fig. 7, we show the equal-time s -wave pair structure factor $S_s(\mathbf{q}, \tau = 0)$ for $|U|/t = 5$ [Fig. 7(a)] for various temperatures ($\beta t = 2 - 10$) on a $2 \times 16 \times 16$ lattice and [Fig. 7(b)] for various system sizes ($L = 10 - 16$) at $T/t = 0.1$. We see that the $\mathbf{q} = 0$ mode becomes more and more singular in both results as we decrease the temperature or increase the system size, which is a characteristic feature of growing s -wave pairing correlations. The dependence of the $\mathbf{q} = 0$ mode on the system size indicates that we need to understand the finite-size scaling behavior of S_s due to

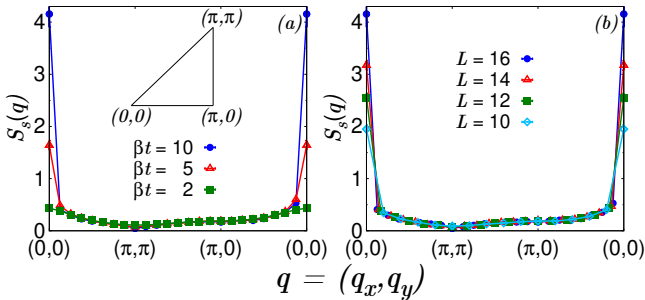


Figure 7. s -wave pair structure factor $S_s(\mathbf{q}, \tau = 0)$ at $|U|/t = 5$ for (a) various temperatures ($\beta t = 2 - 10$) on a $2 \times 16 \times 16$ lattice and (b) various system sizes ($L = 10 - 16$) at $T/t = 0.1$. We see that the $\mathbf{q} = 0$ mode becomes more and more singular in both results as we decrease the temperature or increase the system size.

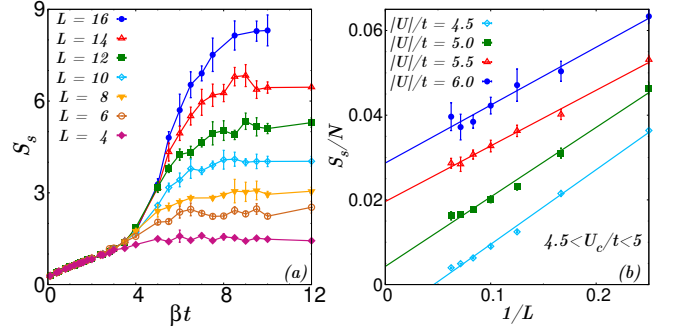


Figure 8. (a) The evolution of the s -wave pair structure factor S_s with the inverse temperature β for different system sizes at $|U|/t = 5$. S_s increases at low temperatures, saturating at a value which increases with the size of the lattice. (b) Ground state: Finite-size scaling of the s -wave pair structure factor for various interaction strengths. The symbols are the DQMC results and the dashed lines are the extrapolation performed via a linear least-squares fit for each $|U|$. We observe that $|U_c|/t \sim 5$.

the limitations on lattice size ($L \leq 16$) imposed by the DQMC algorithm.

Finite-size Scaling

To understand the finite-size scaling behavior of S_s , we obtain the low-temperature limit of the pair structure factor by decreasing the temperature until we observe a plateau which signals that we have reached the $T = 0$ value of the pair structure factor. Figure 8(a) shows the evolution of S_s with the inverse temperature βt for $|U|/t = 5$ and for different lattice sizes. Here we see that S_s increases at low temperatures and saturates to a value which increases with the size of the lattice. For $\beta \leq 4$, pair correlations are short range, so the pair structure factor is independent of the lattice size. As we decrease the temperature, the point at which the pair structure factor begins to grow with the lattice size indicates the temperature at which the correlation length ξ becomes large as compared to the lattice size L .

Ground State: $|U_c|$. The important characteristic of the superfluid state in our bilayer model is that the system displays long-range order in the ground state, and hence Huse's argument [25] of the “spin-wave scaling” is expected to hold [18],

$$\frac{S_s}{N} = \Delta_0^2 + \frac{C(U)}{L} \quad (15)$$

where Δ_0 is the superfluid order parameter at zero temperature and C is a constant which depends on the interaction strength $|U|$.

The superfluid order parameter Δ_0 can also be extracted from the *equal-time* s -wave pair-pair correlation function $P_s(\mathbf{l})$ for the two most distant points on a lattice, i.e., having $\mathbf{R} = (L/2, L/2)$ [26], with a similar spin-wave theory correction,

$$P_s(\mathbf{R}) = \Delta_0^2 + B(U)L. \quad (16)$$

We expect that $B < C$ since the structure factor includes the pair correlations at short distances which markedly

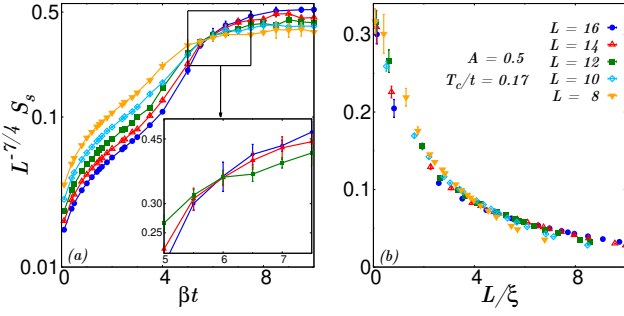


Figure 9. (a) Rescaled S_s as a function of inverse temperature β at $|U|/t = 5$ for different system sizes. The inset shows the enlarged region around $\beta t = 5 - 7.5$. All the curves for different system sizes intercept each other at $\beta t \sim 6$. (b) Rescaled S_s plotted against L/ξ at $|U|/t = 5$ for different system sizes. All the curves for different system sizes collapse to a single curve at $A = 0.5$ and $T_c/t = 0.17$.

exceed Δ_0^2 , in addition to the finite lattice effects at larger length scales [27].

In Fig. 8(b), we perform the finite-size scaling of the s -wave pair structure factor S_s for various interaction strengths. We can approximate the superfluid order parameter by the intercept along the y axis as evident from Eq. (15). Thus we observe that the zero-temperature order parameter is nonzero for the interaction $|U|/t \geq 5$. Hence the critical interaction strength $|U_c|/t \sim 5$.

Estimation of T_c . We can extract T_c from the pair structure factor S_s through a “phenomenological renormalization group” analysis [28, 29]. As we know, $\xi = \infty$ at T_c and $\rightarrow \infty$ for all $0 < T < T_c$ [see Eq. (20)]. Thus, at T_c , $L^{-7/4} S_s(L, \beta_c)$ becomes a constant, independent of the system size. Hence all the curves for different system sizes, in the plot of the rescaled pair structure factor

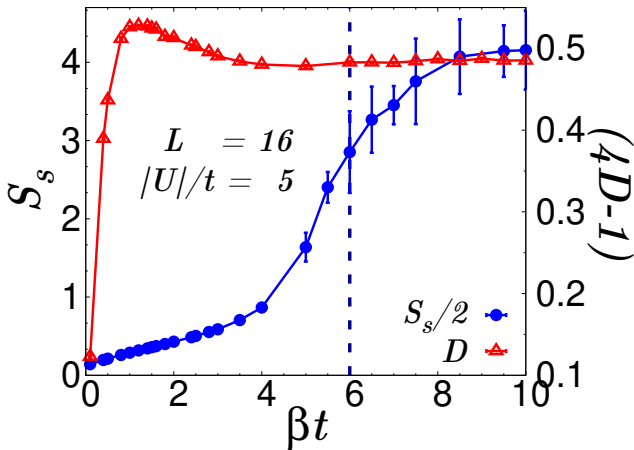


Figure 10. The evolution of the s -wave pair structure factor and the rescaled double occupancy with inverse temperature β at $|U|/t = 5$ and $L = 16$. Two different energy scales are clearly identified. S_s , signaling the emergence of the phase coherence, saturates at $\beta t \sim 8$, whereas \tilde{D} , signaling the molecule formation, saturates at $\beta t \sim 3$.

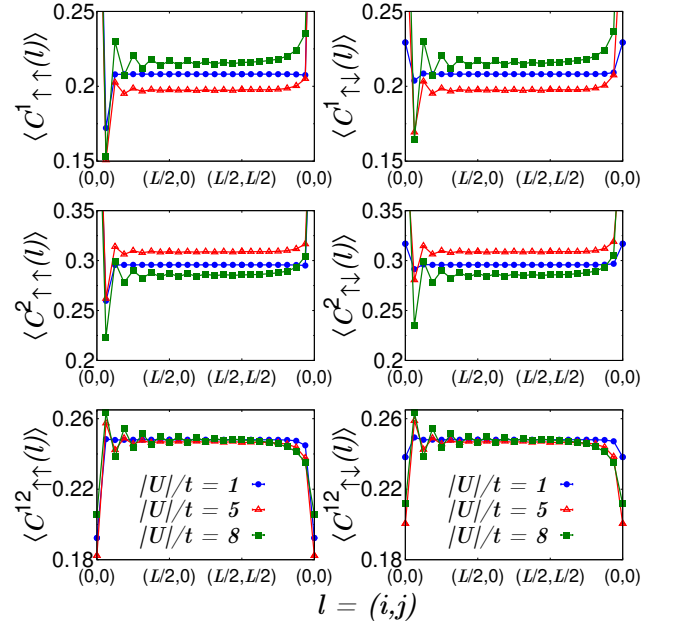


Figure 11. The spatial variation of the density-density correlation function $C_{\sigma, \sigma'}^{\alpha \gamma}(\mathbf{i}, \mathbf{j})$ for different interaction strengths $|U|$ at temperature $T/t = 0.1$ for a system size $N = 512$ sites. It indicates the formation of the spatial density wave pattern for attractive interaction $|U|/t = 8$.

$L^{-7/4} S_s(L, \beta)$, should *intersect* at $\beta = \beta_c$, when plotted as a function of β . In Fig. 9(a), we show the rescaled pair structure factor $L^{-7/4} S_s(L, \beta)$ as a function of the inverse temperature β for $|U|/t = 5$ for different lattice sizes. We observe that for all lattice sizes, all the curves intersect each other at a single point $\beta = 6$. This leads to a conclusion that $T_c/t \sim 0.167$.

In Fig. 9(b), we plot the rescaled pair structure factor versus the universal scaling function $f(L/\xi)$ [see Eq. (20)], where A and T_c are chosen such that all the data points collapse on a single curve, regardless of the system size. For $A = 0.5$ and $T_c/t = 0.17$ at $|U|/t = 5$, all data collapse onto a single curve. Hence the estimated $T_c/t = 0.17$ at $|U|/t = 5$. Similarly, we estimated T_c for various interaction strengths to map out the $T - U$ phase diagram (see Fig. 13).

B. Energy Scales

In our bilayer band-insulator model, we see two different energy scales for the attractive interaction $|U|/t = 5$. One energy scale (T^*/t) corresponds to the formation of molecules, while the other energy scale (T_c/t) corresponds to the emergence of the phase coherence between these pairs. We can identify these two scales by comparing the evolution of the double occupancy and the s -wave structure factor with temperature. In Fig. 10, we show the rescaled double occupancy and the s -wave structure factor for $|U|/t = 5$ for the lattice size $L = 16$. We recover the two energy scales ($T/t \sim 0.125$ corresponding to saturation of S_s and $T^*/t \sim 0.33$ corresponding to the saturation of \tilde{D}) and observe the formation of pairs be-

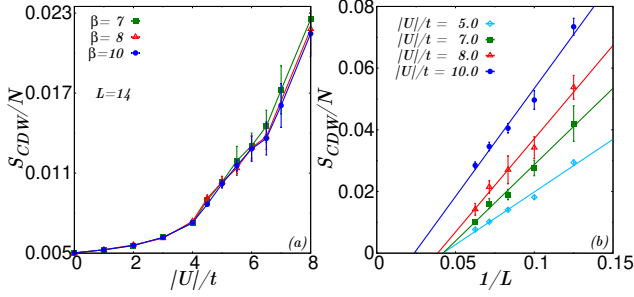


Figure 12. (a) The evolution of the CDW structure factor S_{CDW} with the attractive interaction $|U|$. As the attractive interaction increases the density wave structure factor increases. (b) Finite-size scaling of the CDW structure factor for various interaction strengths. It shows the absence of the charge density wave upto $|U|/t = 10$.

fore the emergence of phase coherence, which is expected in the BEC regime. Finite-size scaling gives $T_c/t \sim 0.17$.

C. Density-Density Correlation

To study the CDW order, we define the density-density correlation function as

$$C_{\sigma,\sigma'}^{\alpha\gamma}(\mathbf{i}, \mathbf{j}) = \langle n_{i\sigma}^{\alpha} n_{j\sigma'}^{\gamma} \rangle - \langle n_{i\sigma}^{\alpha} \rangle \langle n_{j\sigma'}^{\gamma} \rangle \quad (17)$$

where σ and σ' correspond to \uparrow or \downarrow spin, respectively, α and γ correspond to layer A or B , respectively, $n_{i\sigma}^{\alpha}$ corresponds to the fermion density at site i of the α th layer, and i and j run over sites 1 to N . For $\alpha = \gamma$, $C_{\sigma,\sigma'}^{\alpha\gamma}(\mathbf{i}, \mathbf{j})$ corresponds to the intralayer density-density correlation, while for $\alpha \neq \gamma$, $C_{\sigma,\sigma'}^{\alpha\gamma}(\mathbf{i}, \mathbf{j})$ corresponds to the interlayer density-density correlation function. Similarly, we define the CDW structure factor S_{CDW} as

$$S_{CDW}(\mathbf{q}) = \frac{1}{N} \sum_{\alpha\gamma} \sum_{\sigma\sigma'} \sum_{\mathbf{i}\mathbf{j}} e^{i\mathbf{q} \cdot \mathbf{l}_{ij}^{\alpha\gamma}} C_{\sigma,\sigma'}^{\alpha\gamma}(\mathbf{i}, \mathbf{j}) \quad (18)$$

where $\mathbf{l}_{ij}^{\alpha\gamma} = \mathbf{l}(\mathbf{i}, \alpha) - \mathbf{l}(\mathbf{j}, \gamma)$.

In Fig. 11, we show the spatial variation of the density-density correlation function $C_{\sigma,\sigma'}^{\alpha\gamma}(\mathbf{i}, \mathbf{j})$. We observe that the density wave formation will start to take place for $|U|/t \geq 8$. Thus there is no competing order in the region where the superfluid state exists. To confirm this, we perform the scaling analysis.

In Fig. 12(a), we show the evolution of the CDW structure factor S_{CDW} with attractive interaction $|U|$ for various temperatures. S_{CDW} increases slowly in the weak-coupling regime where the system is in a band-insulating state. As the attractive interaction increases, the density wave structure factor increases. To investigate the existence of the charge density wave order in the ground state of the bilayer band-insulating model, we perform the finite-size scaling.

Finite-size Scaling

Using the Huse's argument of the spin-wave theory, we expect that the CDW structure factor and the density-density correlation function behave as

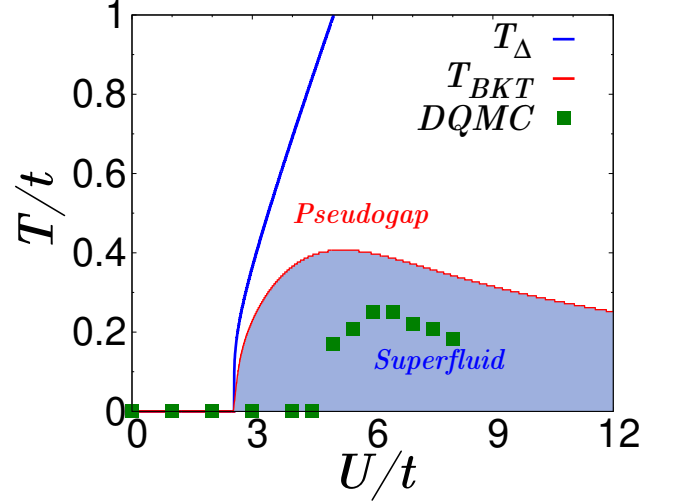


Figure 13. $T - U$ phase diagram. T_{Δ} in the phase diagram represents the pair-breaking temperature obtained through saddle-point analysis, while T_{BKT} refers to the Berezinski-Kosterlitz-Thouless transition temperature of the bilayer model presented in [11]. Square points indicate T_c obtained from the DQMC calculations. We observe that the T_c gets reduced from its mean-field values, as expected. Also, the maximum value of T_c (~ 0.27) occurs at $|U|/t = 6$.

$$\begin{aligned} \frac{S_{CDW}}{N} &= \Delta_0^2 + \frac{C(U)}{L}, \\ C(L/2, L/2) &= \Delta_0^2 + B(U)L, \end{aligned} \quad (19)$$

where Δ_0^2 is the zero-temperature charge density wave order parameter and C and B are constants which depend on the interaction strength $|U|$.

Figure 12(b) shows the finite-size scaling of the CDW structure factor S_{CDW} for various interaction strengths. From Eq. (19) we see that the intercept along the y axis gives the square of the zero-temperature CDW order parameter Δ_0^2 . For the range of attractive interaction strengths (5 – 10), the finite-size scaling of the CDW structure factor confirms that the CDW phase does not exist in the bilayer band-insulating model. Even though we observe density wave formation for $|U|/t \geq 8$, to have a long-range CDW order, the CDW structure factor measured on finite lattices at the critical temperature T'_c should obey

$$L^{-7/4} S_{CDW} \sim f(L(\beta - \beta'_c)), \quad (20)$$

Hence if we plot $L^{-7/4} S_{CDW}$ as a function of the inverse temperature β , different sizes L must cross at $\beta = \beta'_c$. But we could not see any crossing for different system sizes for the CDW structure factor. On the contrary, this crossing has been clearly visible for a pair-pair structure factor where long-range superfluid order is present (Fig. 9). Hence, even for $U/t = 10$, long-range CDW order is absent.

V. DISCUSSION AND CONCLUSION

In summary, we have used an unbiased and exact DQMC technique to study various single-particle

and two-particle properties of the bilayer band-insulator model. We have shown the existence of two energy scales: one scale governs the phase coherence and the other one corresponds to the molecule formation (formation of tightly bound fermionic pairs). We compare our results with the one obtained with the mean-field and the Gaussian-fluctuation theory results presented in [11]. The critical strength $|U_c|/t \sim 5$ is slightly higher than the saddle-point analysis ($|U_c|/t = 3.2$) and is close to the VMC prediction ($|U_c|/t = 4.5$). Through the finite-size scaling, we show that there is no competing CDW order in the bilayer band-insulator model for the interaction range $|U|/t = 5-10$. The saddle-point analysis suggested the maximum critical temperature ~ 0.4 at $|U|/t = 5$, whereas DQMC predicted $T_c/t|_{DQMC} = 0.17$, which is lower than the saddle-point prediction at $|U|/t = 5$. We estimated the transition temperature for various interac-

tion strengths and map out the $T - U$ phase diagram shown in Fig. 13. DQMC simulation predicts the maximum $T_c/t (= 0.27)$ which occurs at $|U|/t \sim 6$. We find that the maximum T_c in our proposed *half-filled* bilayer band insulator is twice that of the maximum $T_c/t \sim 0.13$ (for $|U|/t = 8$) published in Ref. [3] for the single-layer attractive Hubbard model. Thus, the studied bilayer band-insulator model has “higher” characteristic temperature T_c , with no competing orders as compared to earlier attempts, and is expected to be realized in cold-atom experiments.

ACKNOWLEDGEMENTS

Y.P. would like to acknowledge CSIR for financial support. Y.P. thanks A. V. Mallik, A. Halder, and V. B. Shenoy for various discussions and comments. Y.P. would also like to thank V. B. Shenoy for the cluster usage.

-
- [1] P. Nozières and S. Schmitt-Rink, Bose condensation in an attractive fermion gas: From weak to strong coupling superconductivity, *Journal of Low Temperature Physics* **59**, 195 (1985).
 - [2] D. Mitra, P. T. Brown, E. Guardado-Sanchez, S. S. Kondov, T. Devakul, D. A. Huse, P. Schauß, and W. S. Bakr, Quantum gas microscopy of an attractive fermi-hubbard system, *Nature Physics* **14**, 173 (2018).
 - [3] R. T. Scalettar, E. Y. Loh, J. E. Gubernatis, A. Moreo, S. R. White, D. J. Scalapino, R. L. Sugar, and E. Dagotto, Phase diagram of the two-dimensional negative- U Hubbard model, *Physical Review Letters* **62**, 1407 (1989).
 - [4] T. Paiva, R. Scalettar, M. Randeria, and N. Trivedi, Fermions in 2d optical lattices: Temperature and entropy scales for observing antiferromagnetism and superfluidity, *Phys. Rev. Lett.* **104**, 066406 (2010).
 - [5] R. A. Fontenele, N. C. Costa, R. R. dos Santos, and T. Paiva, Two-dimensional attractive hubbard model and the bcs-bec crossover, *Phys. Rev. B* **105**, 184502 (2022).
 - [6] T.-L. Ho and Q. Zhou, Squeezing out the entropy of fermions in optical lattices, *Proceedings of the National Academy of Sciences* **106**, 6916 (2009).
 - [7] T.-L. Ho and Q. Zhou, Universal cooling scheme for quantum simulation, *arXiv:0911.5506*.
 - [8] J.-S. Bernier, C. Kollath, A. Georges, L. De Leo, F. Gerbier, C. Salomon, and M. Köhl, Cooling fermionic atoms in optical lattices by shaping the confinement, *Physical Review A* **79**, 061601(R) (2009).
 - [9] D. C. McKay and B. DeMarco, Cooling in strongly correlated optical lattices: prospects and challenges, *Reports on Progress in Physics* **74**, 054401 (2011).
 - [10] M. Gall, C. F. Chan, N. Wurz, and M. Köhl, Simulating a mott insulator using attractive interaction, *Phys. Rev. Lett.* **124**, 010403 (2020).
 - [11] Y. Prasad, A. Medhi, and V. B. Shenoy, Fermionic superfluid from a bilayer band insulator in an optical lattice, *Phys. Rev. A* **89**, 043605 (2014).
 - [12] A. Halder and V. B. Shenoy, Cooling a band insulator with a metal: Fermionic superfluid in a dimerized holographic lattice, *Scientific Reports* **4**, 6655 (2014).
 - [13] M. Kohmoto and Y. Takada, Superconductivity from an insulator, *Journal of the Physical Society of Japan* **59**, 1541 (1990).
 - [14] P. Nozières and F. Pistolesi, From semiconductors to superconductors: a simple model for pseudogaps, *The European Physical Journal B-Condensed Matter and Complex Systems* **10**, 649 (1999).
 - [15] A. Moreo and D. J. Scalapino, Two-dimensional negative- U Hubbard model, *Physical Review Letters* **66**, 946 (1991).
 - [16] R. R. dos Santos, Second-neighbor hopping in the attractive Hubbard model, *Physical Review B* **46**, 5496 (1992).
 - [17] B. Kyung, S. Allen, and A. M. S. Tremblay, Pairing fluctuations and pseudogaps in the attractive Hubbard model, *Physical Review B* **64**, 075116 (2001).
 - [18] T. Paiva, R. R. dos Santos, R. T. Scalettar, and P. J. H. Denteneer, Critical temperature for the two-dimensional attractive Hubbard model, *Physical Review B* **69**, 184501 (2004).
 - [19] A. Zujev, R. T. Scalettar, G. G. Batrouni, and P. Sen Gupta, Pairing correlations in the two-layer attractive Hubbard model, *New Journal of Physics* **16**, 013004 (2014).
 - [20] R. Blankenbecler, D. J. Scalapino, and R. L. Sugar, Monte Carlo calculations of coupled boson-fermion systems. I, *Physical Review D* **24**, 2278 (1981).
 - [21] R. R. d. Santos, Introduction to quantum Monte Carlo simulations for fermionic systems, *Brazilian Journal of Physics* **33**, 36 (2003).
 - [22] R. Jordens, N. Strohmaier, K. Gunter, H. Moritz, and T. Esslinger, A Mott insulator of fermionic atoms in an optical lattice, *Nature(London)* **455**, 204 (2008).
 - [23] V. L. Berezinskii, Destruction of long-range order in one-dimensional and two-dimensional systems possessing a continuous symmetry group. ii. quantum systems, *Russian Journal of Experimental and Theoretical Physics* **34**, 610 (1972).
 - [24] J. M. Kosterlitz and D. J. Thouless, Ordering, metastability and phase transitions in two-dimensional systems,

- [Journal of Physics C: Solid State Physics](#) **6**, 1181 (1973).
- [25] D. A. Huse, Ground-state staggered magnetization of two-dimensional quantum Heisenberg antiferromagnets, [Physical Review B](#) **37**, 2380 (1988).
- [26] R. T. Scalettar, N. Trivedi, and C. Huscroft, Quantum Monte Carlo study of the disordered attractive Hubbard model, [Physical Review B](#) **59**, 4364 (1999).
- [27] C. N. Varney, C.-R. Lee, Z. J. Bai, S. Chiesa, M. Jarrell, and R. T. Scalettar, Quantum Monte Carlo study of the two-dimensional fermion Hubbard model, [Physical Review B](#) **80**, 075116 (2009).
- [28] P. Nightingale, Finite-size scaling and phenomenological renormalization, [Journal of Applied Physics](#) **53**, 7927 (1982).
- [29] R. R. dos Santos and L. Sneddon, Finite-size rescaling transformations, [Physical Review B](#) **23**, 3541 (1981).